TRANSNAV
http://www.transnav.eu
the International Journal
on Marine Navigation
and Safety of Sea Transportation
Volume 14
Number 2
June 2020

DOI: 10.12716/1001.14.02.08

# Edge Element Calculation of Radar Cross Section of Small Maritime Targets with Respect to Height of Radar Antenna

H. Dodig, S. Vukša & P. Vidan
*University of Split, Split, Croatia*

M. Bukljaš
*University of Zagreb, Zagreb, Croatia*

ABSTRACT: From the aspect of navigational safety and collision avoidance it is very important to be able to detect small maritime targets such as buoys and small boats. Ship's radar is supposed to detect these types of targets, however the ability of radar to detect such targets depends on several factors. The most important factors affecting the detection probability of small maritime targets are height of the antenna installation on the ship and radar cross section of the target. The methods of computation radar cross section are diverse and complicated, however, in this paper we apply our previously published numerical method for the RCS computation which had proven to be very accurate. Physically to find RCS of the target one has to find the solution of electromagnetic scattering problem. The numerical method relies on the combination of finite edge volume elements and finite edge boundary elements to obtain the solution of Maxwell equations. The radiation pattern of ships radar antenna is the source of excitation for the numerical method. At the end of the paper the RCS of small maritime targets as the function of antenna height is shown. These results can be used as a parameter in radar design, as well as the guideline for the height of installation of the ship's radar antenna above the sea.

## 1 INTRODUCTION

The detection of small vessels with insignificant radar scattering cross section (RCS) is of crucial importance for navigation safety when navigating in coastal waters with dense maritime traffic such as near tourist destinations with large tourist populations during summer season. This is especially true for indented coasts with numerous islands and deep coves such as Croatian coast. With these circumstances, the ability to detect small vessels at short ranges determines safety of navigation, especially during night and in bad weather conditions. Situation is additionally worsened by the typical material composition of these small vessels since plastic, wood and rubber do not contribute to RCS as much as metal parts. For that reason, this paper concerns with the numerical computation of RCS of the small rubber boat.

Radar installations on ships navigating these waters vary from small radars installed on small vessels with typical power output of 4kW (e.g. Garmin) to 25kW marine radars typically installed on larger passenger vessels such as ferry-boats. Many ship captains have reported the inability to reliably detect fast approaching rubber boat with radar which, additionally, is difficult to distinguish from sea clutter. Thus, in this paper, we attempt not to improve radar itself but we rather numerically investigate the possibility of finding the optimal height of radar installation above the sea line to maximize the possibility of radar detection of rubber boat.

Numerical methods available for RCS computation generally fall in one of three distinct categories: ray-tracing methods, physical optics methods and full wave methods. Ray tracing methods are often complicated because multibouncing of rays need to be taken into account (Liu, 2012). Furthermore, ray tracing methods do not take into account the changing electromagnetic properties of the materials used for interior of the vessel. Methods such as physical optics (PO) and physical theory of diffraction (PTD) can compute RCS with acceptable error, however these methods are not well suited for accounting the changing material properties in the interior of the ship.

Thus, if we were to account for changing material properties inside the vessel we can use one of the following: FDTD (finite difference method), some hybrid combination of method of moments (MoM) with finite element method (FEM). However, these methods can only provide near field solution of electromagnetic scattering problem and they need to be subjected to near-to-far field transformation (NTFFT) in order to compute RCS which is cumbersome procedure (Taflove, 2005).

To avoid NTFFT transform, in this research we use our own previously published method for RCS computation based on hybrid BEM/FEM with edge elements (Dodig, 2017). This method first finds the near field solution and from these electromagnetic field values, using our own RCS equation, we compute RCS directly from near field values. Thus, the NTFFT transformation is avoided and sometimes this approach produces better results (e.g. the case of RCS computation at interior resonance frequencies, see. Dodig, 2017).

The results of the numerical computation of RCS are presented in section 5, where RCS is expressed as the function of the angle between the line of sight connecting radar antenna and rubber boat and the sea level. It is shown that detection probability of the rubber boat is very angle dependent for vertical polarization and that in order to maximize the detection probability of rubber boat at certain distance the radar antenna should be placed at some definite height above the sea level.

## 2 NEAR FIELD COMPUTATION WITH EDGE ELEMENT HYBRID BEM/FEM

To compute the RCS of radar target the necessary step is the computation of backscattered electric and magnetic field at the exterior boundary of the computational problem shown in figure. This computed backscattered EM field is the near field solution of EM scattering problem and, as such does not represent the far field data necessary for RCS computation.

In order to obtain the near field solution one needs to obtain the solution of general 3D electromagnetic scattering problem. This general 3D scattering problem is shown in figure 1, where incident electric and magnetic fields are denoted as $\vec{E}_i$ and $\vec{H}_i$, backscattered fields are denoted $\vec{E}_S$ and $\vec{H}_S$ and interior fields are denoted $\vec{E}_{int}$ and $\vec{H}_{int}$. Interior and backscattered electromagnetic fields are the fields we wish to compute, while the incident electric and magnetic fields are known, and in the case of the computation of ship's RCS they come from radar antenna. Because the electromagnetic properties of materials ($\epsilon_r, \mu_r, \sigma$) change inside computational domain $V$, we need to use computational method that can take these changes into account.

The method of computational electromagnetism that can take into account the change of these electromagnetic properties is hybrid BEM-FEM, which is the combination of boundary element method (BEM) and finite element method (FEM), and the method is thoroughly described in ref. Dodig 2012-2014. Electric field exterior to computational boundary $\partial V$, shown in figure 1, can be described by Stratton-Chu electric field integral equation (EFIE) which in its time harmonic form can be written as (e.g. Stratton 1939):

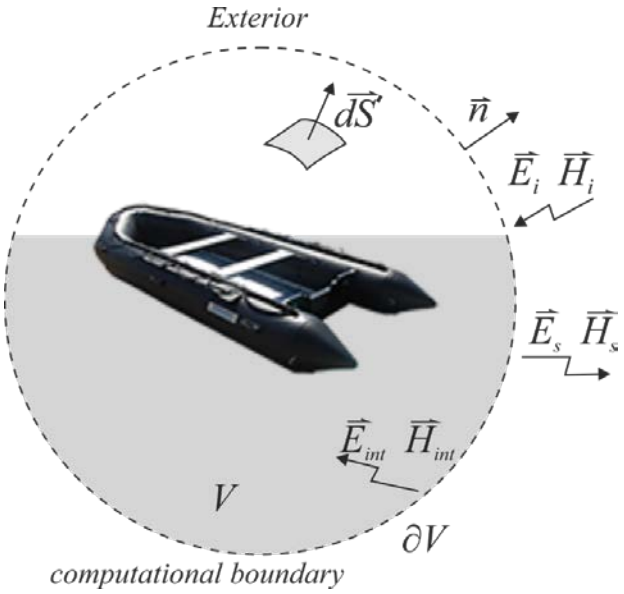


Figure 1. Outline of EM scattering problem. Volume of computational domain is denoted $V$ and the artificial boundary is denoted $\partial V$. Fields $\vec{E}_i$ and $\vec{H}_i$ are incident to $\partial V$ while $\vec{E}_S$ and $\vec{H}_S$ are backscattered fields.

$$\alpha\vec{E}_{ext} = \vec{E}_i - i\omega\mu\oint_{\partial V} d\vec{S}' \times \vec{H}'_{ext} G + \oint_{\partial V} \left(d\vec{S}' \times \vec{E}'_{ext}\right) \times \nabla' G - \oint_{\partial V} dS' \frac{1}{\sigma + i\omega\epsilon} \nabla' \cdot \left(\vec{n}' \times \vec{H}'_{ext}\right) \nabla' G \quad (1)$$

For interior fields, that is for electromagnetic fields inside computational volume $V$ shown in figure 1, the time harmonic Faraday's law takes the following mathematical form:

$$\nabla' \times \vec{\mathrm{E}}'_{int} = -i\omega\mu\vec{\mathrm{H}}'_{int} \quad (2)$$

and time harmonic Maxwell-Ampere equation is given by:

$$\nabla' \times \vec{\mathrm{H}}'_{int} = \left(\sigma + i\omega\epsilon\right)\vec{\mathrm{E}}'_{int} \quad (3)$$

Taking the curl of Equation 3 and combining with Equation 2 yields the following differential equation:

$$\nabla\times\left(\frac{1}{\sigma+\mathrm{i}\omega\epsilon}\nabla'\times\vec{\mathrm{H}}_{int}^{'}\right)+i\omega\mu\vec{\mathrm{H}}_{int}^{'}=0 \tag{4}$$

With computational methods for electrostatics the unknown fields $\vec{\mathrm{E}}_{int}^{'}$ and $\vec{\mathrm{H}}_{int}^{'}$ are usually approximated with nodal approximating functions. However, that is not appropriate for full wave methods. With full wave methods we use edge element approximating functions in order to preserve the continuity of tangential components of electric and magnetic fields (see Dodig 2017 for details). Edge elements approximate electric and magnetic fields using vector approximating functions $\vec{w}_i$ as:

$$\vec{\mathrm{E}}_{int}=\sum_{i=1}^{n}\delta_i\vec{w}_i e_i \tag{5}$$

$$\vec{\mathrm{H}}_{int}=\sum_{i=1}^{n}\delta_i\vec{w}_i h_i \tag{6}$$

where $n$ is the number of edges on the element, $e_i$ and $h_i$ are unknown coefficients associated with each edge of the element. Vector approximating functions $\vec{w}_k$ are associated with $k^{th}$ edge of the element by the following relation:

$$\vec{w}_k=N_i\nabla N_j-N_j\nabla N_i \tag{7}$$

where $N_i$ and $N_j$ are nodal approximating functions associated with nodes of the element (Nedelec, 1980).

Due to physical jump conditions of electric and magnetic fields at the interface between two materials with different electromagnetic properties, all the exterior fields in Equation 1 i.e. $\vec{\mathrm{E}}_{ext}$ and $\vec{H}_{ext}^{'}$, can be replaced by interior fields $\vec{\mathrm{E}}_{int}$ and $\vec{H}_{int}^{'}$. This is due to tangential continuity of electric and magnetic fields across the boundary where material properties change. With these conditions, Equation 1 and Equation 4 can be coupled and combining with Equations 5 – 7 the following system of equations is obtained:

$$\begin{bmatrix} G & -H & 0\\ -D & F & F\\ 0 & F & F\end{bmatrix}\begin{Bmatrix} e_b\\ h_b\\ h_v\end{Bmatrix}=\begin{Bmatrix} e_I\\ 0\\ 0\end{Bmatrix} \tag{8}$$

where $e_I$ are edge element coefficients computed from incident field $\vec{\mathrm{E}}_{\mathrm{i}}$, $e_b$ and $h_b$ are edge element coefficients associated with edges at the artificial boundary $\partial V$ and $h_v$ are edge element coefficeints associated with interior of the computational domain $V$. The hybrid BEM-FEM method of numerical computation of near electromagnetic field was rigorously tested over the period of several years in various physical settings (Dodig 2012-2017 and Cvetković 2017).

## 3 NUMERICAL METHOD OF RADAR CROSS SECTION COMPUTATION

Radar cross section is computed directly from the edge element coefficients computed in previous section. These coefficients are associated with near electric and magnetic field, that is, the near electromagnetic field can be reconstructed from edge element coefficients (Dodig 2017). To compute radar cross section, one has to convert the near field to far field. Previously, this transformation from near field to far field was achieved by the employment of some elaborate and computationally expensive numerical methods (Taflove 2005). These methods are collectively known as Near-to-Far-Field-Transformation (NFFT).

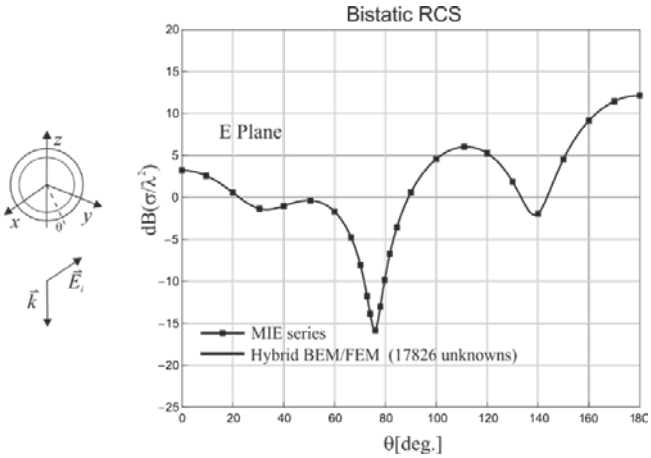


Figure 2. RCS plot of the metallic sphere coated with dielectric layer with relative permittivity $\epsilon_r=4$. This calculation was performed using EFIE formulation and hybrid BEM/FEM at resonant frequency of 300 MHz and was compared with Mie series solution.

The necessity for NFFT can be circumvented completely and far field can be computed directly from edge element coefficients by the application of our previously published computational technique (Dodig 2017). Radar cross scattering section $\sigma$ is defined as ratio of backscattered and incident field:

$$\sigma=\lim_{|\vec{r}|\to\infty}4\pi|\vec{r}|^2\frac{\left|\vec{E}_S\right|^2}{\left|\vec{E}_i\right|^2}=\lim_{|\vec{r}|\to\infty}4\pi|\vec{r}|^2\frac{\vec{E}_S\cdot\vec{E}_S^{*}}{\vec{E}_I\cdot\vec{E}_I^{*}} \tag{9}$$

where $\vec{E}_S^{*}$ represents the complex conjugate of backscattered vector field $\vec{E}_S$. It was shown in ref. Dodig 2017 that this backscattered field can be written in compact form as:

$$\vec{E}_S=\frac{e^{-ik|\vec{r}|}}{4\pi|\vec{r}|}\vec{F}_S \tag{10}$$

where complex vector $\vec{F}_S$ can elegantly be computed from edge element coefficients as the sum:

$$\vec{F}_S\left(\vec{e}_\rho\right) = -i\omega\mu\sum_{i=1}^{N}\sum_{j=1}^{3}\int_{\Delta_i} h_{bj} e^{ik\vec{r}'\cdot\vec{e}_\rho} d\vec{S}' \times \delta_j \vec{w}_j +$$

$$ik\sum_{i=1}^{N}\sum_{j=1}^{3}\int_{\Delta_i} e_{bj} e^{ik\vec{r}'\cdot\vec{e}_\rho}\left(d\vec{S}' \times \delta_j \vec{w}_j\right) \times \qquad (11)$$

$$\vec{e}_\rho - ik\sum_{i=1}^{N}\sum_{j=1}^{3}\int_{\Delta_i} h_{bj} e^{ik\vec{r}'\cdot\vec{e}_\rho} dS' \frac{\nabla'_S \cdot \left(\vec{n}' \times \vec{w}_j\right)}{\sigma + i\omega\epsilon}\vec{e}_\rho$$

Computation of $\vec{F}_S\left(\vec{e}_\rho\right)$ from known boundary edge coefficients $e_{bj}$ and $h_{bj}$ is fast, and if necessary, the line integrals in Equation 11 can be solved analytically to further improve the speed and accuracy of RCS calculation. Equations 9 – 11 are well tested on canonical models, were compared with Mie series analytical solutions and were tested in the case of dielectrically coated PEC sphere (e.g. Dodig 2017) where it has been shown that accurate results can be obtained even at resonance frequencies as shown in figure 2.

## 4 PHYSICAL AND GEOMETRICAL MODEL OF RUBBER BOAT

From the standpoint of collision avoidance and from standpoint of early detection of small targets in military missions, the rubber boat is considered as the radar target of choice. The rubber boat model used for numerical RCS computation is the model of small service boat usually attached to Croatian Navy ships for the support of some small scale off-ship military missions. The rubber boat was subjected to series of 3D laser measurements to accurately capture the geometry of the boat, as shown in figure 3.

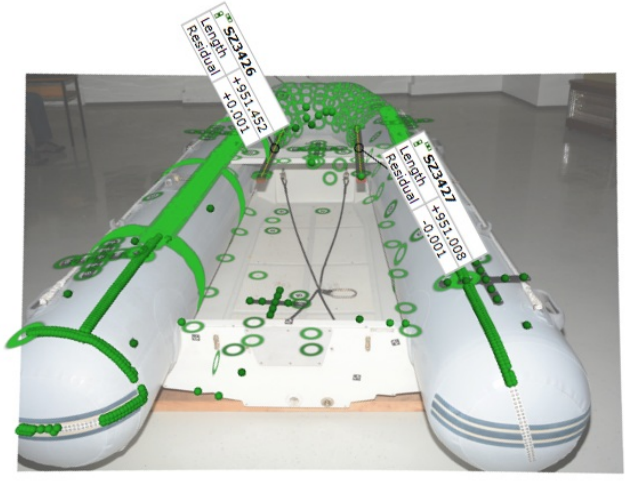


Figure 3. Photo of the rubber boat at laser measurement site. The relevant geometric features of the boat are captured at spatial points marked with green dots.

Geometry capture software produced the set of 3D points and set of linear triangles from laser measurements, conveniently given in the form of STL (stereolitography) file. However, to produce the mesh of good quality with Ansys ICEM software the parasolid or similar input file is required. For that purpose, Geomagic software was used to convert from STL file to Parasolid x_t format and then the air and water volume surrounding the boat were added with Siemens SolidEdge CAD software as shown in figure 4.

CAD model of the rubber boat was loaded into Ansys ICEM mesher to produce the tetrahedral mesh shown in figure 5, where the volume of the air was removed to enhance the visibility of interior elements.

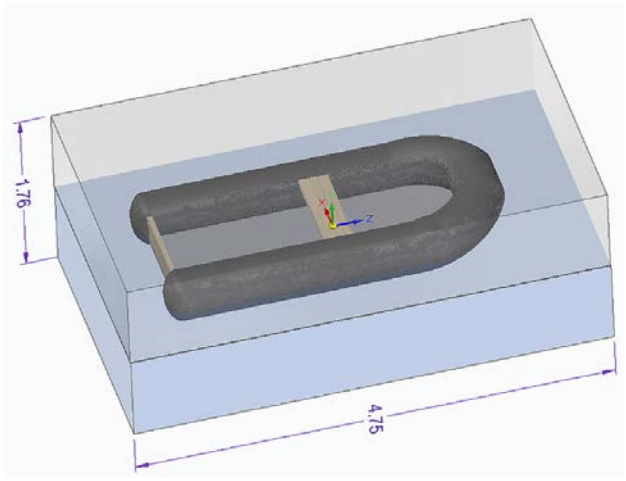


Figure 4. CAD model of the geometry for RCS computation. Upper half of the volume consists of air and the lower half of the volume consists of seawater. Rubber boat is partially immersed in water and partially immersed in air.

Final computational models consists of 285,064 tetrahedral elements and of 1,870 triangular elements used to model the boundary of the computational model.

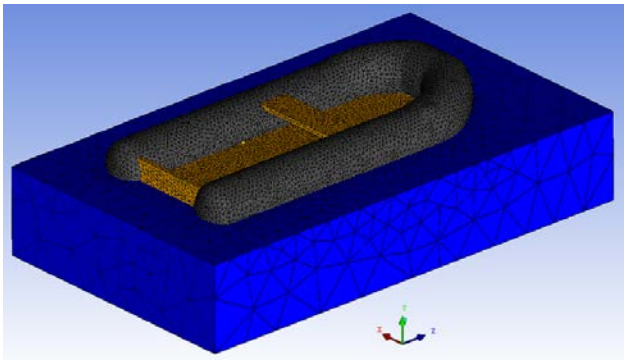

Figure 5. The mesh of the model shown in figure 4 with air volume removed. The model consists of 286,934 elements where 285,064 tetrahedral elements were used to model the interior of computational domain and 1,870 elements were used to model the boundary of computational domain.

Electrical parameters $\sigma, \epsilon_r, \mu_r$ of the seawater, air, rubber and plastic were compiled from various sources from literature (e.g. Talley 2011, Garazza 2011) and these are shown in table 1.

Table 1. Electrical properties $\sigma, \epsilon_r, \mu_r$ of the materials used for RCS computation compiled from various sources.

| **Physical property** | $\sigma$ [S/m] | $\epsilon_r$ | $\mu_r$ |
|---|---|---|---|
| Seawater | 0.00 | 88.00 | 1.00 |
| Air | 0.00 | 1.00 | 1.00 |
| Rubber | 0.00 | 2.50 | 1.00 |
| Plastic | 3.00 | 3.00 | 1.00 |

## 5 RESULTS OF RCS COMPUTATION

Physical setting for RCS computation is shown in figure 6, where the rubber boat is at distance $l$ from the ship and radar antenna is at height $h$ above the sea level. The angle between the line connecting the radar antenna and rubber boat and the sea level is $\theta$.

Furthermore, it is assumed that sea is at calm state. Horizontal polarization (HP) and vertical polarization (VP) of the radar EM wave are shown in the same figure and $\vec{k}$ indicates the direction of propagation of radar EM wave.

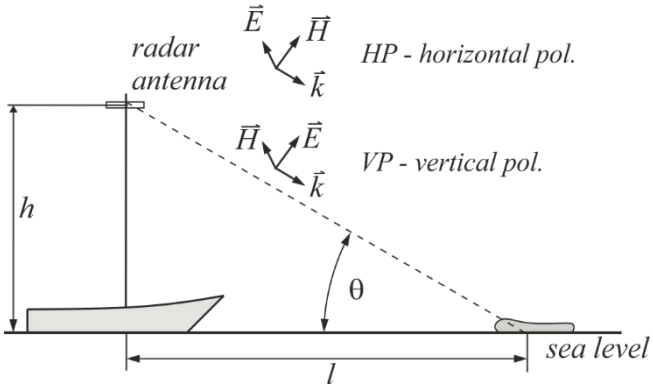


Figure 6. The rubber boat is at horizontal distance $l$ from the radar antenna and the radar antenna is at height $h$ above sea level. Angle subtended between the line connecting the antenna an boat and between sea level is $\theta$.

To find the radar cross section $\sigma_S$ of the sea without the rubber boat we have first performed the series of calculations for the physical setup shown in figure 6 but without rubber boat. The results of numerical radar cross section calculation of $\sigma_S$ for various angles $\theta$ is shown in figure 7 for both HP and VP.

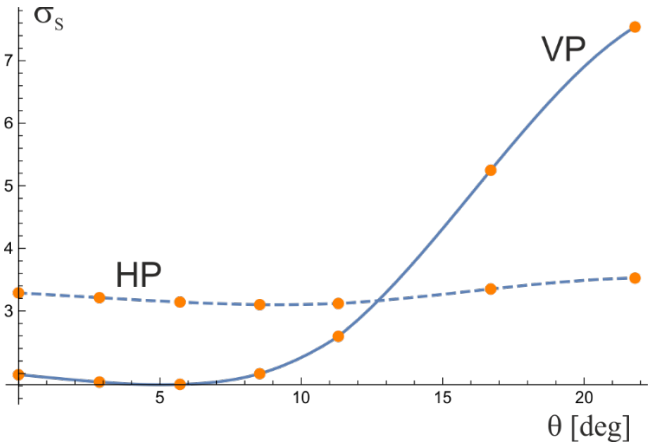


Figure 7. Radar cross sections $\sigma_S$ of the empty sea at calm state without rubber boat for various angles $\theta$ are shown for both HP and VP.

Then the same series of numerical calculations is performed for the configuration shown in figure 6 with the rubber boat included. This time, the radar cross section $\sigma$ is the total cross section that includes reflections from both the sea and from rubber boat. These results are shown in figure 8.

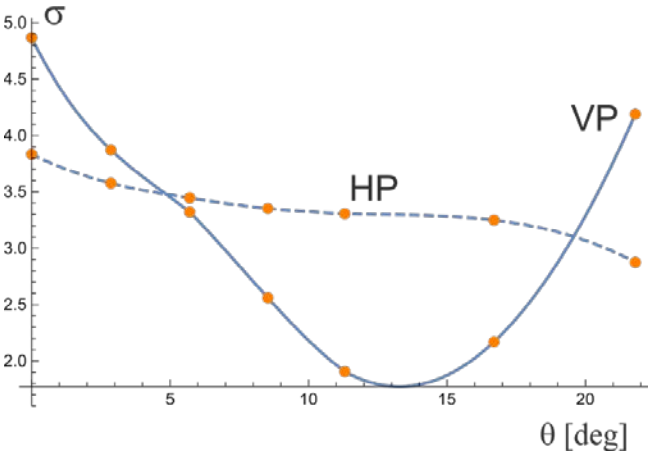


Figure 8. Radar cross section $\sigma$ of the rubber boat and the sea at calm state as the function of angle $\theta$ is shown for both HP and VP.

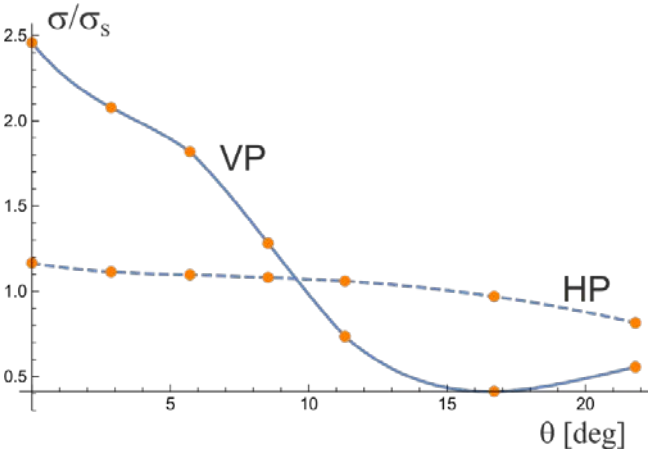


Figure 9. The ratio of cross section $\sigma / \sigma_S$ is shown as the function of angle $\theta$ is shown for both HP and VP. The sea state is considered to be calm.

The reason why these calculations were performed separately (without rubber boat and with rubber boat) is to find how much radar cross section of the rubber boat distinguishes itself from the radar cross section of the sea. The ratio $\sigma / \sigma_S$ shows how much radar cross section of the rubber boat is above the radar cross section $\sigma_S$ of the empty sea and is shown in figure 9.

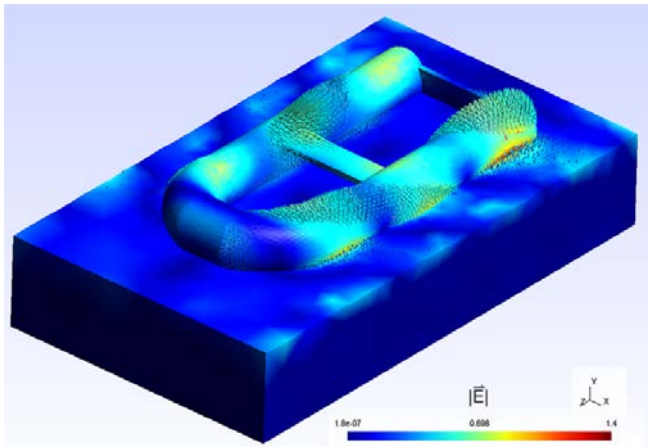


Figure 10. Magnitude and vector plot of near electric field with air omitted for $\theta = 3^{\circ}$, horizontal polarization (HP).

## 6 CONCLUSION

RCS of the rubber boat is computed for physical setting shown in figure 6 for various angles $\theta$ and for both vertical and horizontal polarization of the radar EM wave. For numerical computation of near field we have used hybrid BEM/FEM with edge elements. The results of near field computation were used as input for our own RCS computational method which uses this values directly without the need for NTFFT transformation. This method falls in the class of the full wave methods and it can account for the change of electric and magnetic properties of materials inside the computational domain. An example of near field computation for $\theta = 3^{\circ}$ and horizontal polarization is shown in figure 10.

To be able to distinguish the radar cross section of the sea and of the rubber boat we have first computed the RCS of the sea patch without the rubber boat and these results are shown in figure 7. Then we have computed total RCS of both rubber boat and sea as shown in figure 8. The measure of how much rubber boat is distinguished from the RCS of the sea itself is shown in figure 9. This measure is expressed as simple ratio between RCS of the sea and RCS of both sea and rubber boat.

It should be noted that from figure 9 it follows that the detectability of the rubber boat differs for vertical polarization (VP) and horizontal polarization (HP). From figure 9 it follows that detectability of rubber boat for horizontal polarization (HP) is approximately constant for the range of angles $\theta$. However, for vertical polarization the detectability of rubber boat varies significantly with angle $\theta$.

Furthermore, the capabilities of our RCS computational software are currently limited with two limitations: the size of computational model (the number of unknowns) and with computational time. Currently, an effort is underway to address these issues so that much larger ship models could be used for RCS computation.

## REFERENCES


Liu J., Fang N., Wang B. & Zhang L. 2012. An efficient ray-tracing method for RCS prediction in GRECO, *Microw. Opt. Technol. Lett.* 55(3): 586–589.

Taflove A. & Hagness S. C. 2005. *Computational Electrodynamics*, Boston: Artech House Inc.

Dodig, H., Poljak D. & Peratta A. 2012. Hybrid BEM/FEM edge element computation of the thermal rise in the 3D model of the human eye induced by high frequency EM waves, *Proc. of SOFTCOM 2012*.

Dodig, H., Lalléchère S., Bonnet P., Poljak. D. & Khamlichi El. 2014. Stochastic sensitivity of the electromagnetic distributions inside a human eye modeled with a 3D hybrid BEM/FEM edge element method, *Eng. Anal. Bound. Elem.* 49: 48–62.

Dodig, H. 2017. A boundary integral method for numerical computation of radar cross section of 3D targets using hybrid BEM/FEM with edge elements, *J. Comput. Phys.* 348: 790–802.

Stratton J. & Chu L.J. 1939, Diffraction theory of electromagnetic waves, *Phys. Rev.* 56: 99-107.

Nedelec J.C. 1980. Mixed finite elements in R3, Numer. Math. 35: 315-341.

Cvetković M., Dodig H. & Poljak D. 2017. A Study on the use of compound and extracted models in the high frequency electromagnetic exposure assessment, Math. Probl. Eng., open access, online, Volume 2017, Article ID 7932604.

Talley L.D., Pickard G.L., Emery W.J. & Swift J.H. 2011. *Descriptive physical oceanography*, New York: Elsevier.

Garazza A.R.L, Sorichetti P., Marzocca A.J. & Monti G.A. 2011. Influence of the microstructure of vulcanized polybutadiene rubber on the dielectric properties. *Polym. Test.* 30:657-662.